Accurate Localization of Tagged Objects Using Mobile RFID-Augmented Robots

Xiulong Liu, Jiuwu Zhang, Shan Jiang, Yanni Yang, Keqiu Li, Jiannong Cao, *Fellow, IEEE*, and Jiangchuan Liu, *Fellow, IEEE*

Abstract—This paper studies the problem of tag localization using RFID-augmented robots, which is practically important for promising warehousing applications, e.g., automatic item fetching and misplacement detection. Existing RFID localization systems suffer from one or more of following limitations: requiring specialized devices; only 2D localization is enabled; having blind zone for mobile localization; low scalability. In this paper, we use Commercial Off-The-Shelf (COTS) robot and RFID devices to implement a Mobile RF-robot Localization (MRL) system. Specifically, when the RFID-augmented robot moves along the straight aisle in a warehouse, the reader keeps reading the target tag via two vertically deployed antennas ($\mathcal{R}_1$ and $\mathcal{R}_2$) and returns the tag phase data with timestamps to the server. We take three points in the phase profile of antenna $\mathcal{R}_1$ and leverage the spatial and temporal changes inherent in this phase triad to construct an equation set. By solving it, we achieve the location of target tag relative to the trajectory of antenna $\mathcal{R}_1$. Based on different phase triads, we can have candidate locations of the target tag with different accuracy. Then, we propose theoretical analysis to quantify the deviation of each localization result. A fine-grained localization result can be achieved by assigning larger weights to the localization results with smaller deviations. Similarly, we can also calculate the relative location of target tag with respect to the trajectory of antenna $\mathcal{R}_2$. Leveraging the geometric relationships among target tag and antenna trajectories, we eventually calculate the location of target tag in 3D space. We perform various experiments to evaluate the performance of the MRL system and results show that the proposed MRL system can achieve high accuracy in both 2D and 3D localization.

Index Terms—RFID, mobile robot, localization, phase profile

1 Introduction

1.1 Background and Problem Statement

In the future smart warehousing scenarios, robots may completely replace human beings in terms of automatic object fetching and delivery. Indoor localization is one of the most important techniques for realizing this vision. In fact, a batch of techniques, such as GPS [1], wireless sensor [2], [3], [4], [5], [6], [7], bluetooth [8], Wi-Fi [9], [10] and computer vision [11], have been proposed. However, none of these techniques is suitable for large-scale warehousing scenarios due to the following reasons: (1) The GPS technique works well for the outdoor localization and navigation, but fails in the indoor scenarios; (2) The techniques based on wireless sensors and bluetooth beacons cannot provide a long-term localization service due to the limited volume of batteries; (3) The WiFi-based tracking techniques exploit signal reflection to locate objects but fail to distinguish similar objects; (4) The computer vision-based approaches require line-of-sight between the target objects and camera. Compared with the above techniques, Radio Frequency Identification (RFID) naturally has various advantages including low cost, easy deployment, battery-free, individual identification and no requirement on line-of-sight [12], [13], [14], [15], [16]. Hence, RFID technique has promising prospects for object localization in large-scale warehousing scenarios [17], [18], [19], [20], [21], [22], [23], [24], [25], [26], [27], [28].

The studied problem is localization of tagged objects using a mobile RFID-augmented robot, which is formulated as follows. *As illustrated in Fig. 1, an RFID-augmented robot moves along a straight aisle in a warehouse. The RFID reader on the robot keeps reading the nearby tags via two vertically deployed antennas and the collected RFID data (i.e., tag IDs, phase values, antenna port, and timestamps) will be forwarded to the server embedded in robot or remote server via WiFi connection. The point where the below antenna $\mathcal{R}_1$ starts to move is regarded as point $O(0,0,0)$; The X–axis is parallel to the moving direction of the mobile robot; The Y–axis is perpendicular to the X–axis and parallel to the ground plane; The Z–axis is upward perpendicular to the ground plane. The server leverages the collected RFID data to calculate the locations of the target objects in the 3D coordinate system.*

1.2 Limitations of Prior Art

Although considerable efforts were made by research communities to solve the problem of RFID localization, existing localization systems [23], [24], [29], [30], [31], [32], [33] still suffer from one or more of the following limitations. *Requiring specialized devices*: The AoA [31] system and PinIt system [32] require specialized devices, e.g., USRP and self-designed

- *X. Liu, J. Zhang, and K. Li are with the College of Intelligence and Computing, Tianjin University, Tianjin 300072, China. Partial work of Xiulong Liu was done at SFU as a postdoctoral fellow under supervision of Prof. Jiangchuan Liu. E-mail: xiulongliudut@gmail.com, {zhangjiuwu, keqiu}@tju.edu.cn.*
- *S. Jiang, Y. Yang, and J. Cao are with the Department of Computing, Hong Kong Polytechnic University, Hong Kong, China. E-mail: {cssjiang, csynyang}@comp.polyu.edu.hk, jiannong.cao@polyu.edu.hk.*
- *J. Liu is with the School of Computing, Simon Fraser University, Burnaby, BC V5A 1S6, Canada. E-mail: jcliu@cs.sfu.ca.*

Manuscript received 25 July 2019; revised 6 Nov. 2019; accepted 10 Dec. 2019. Date of publication 24 Dec. 2019; date of current version 4 Mar. 2021. (Corresponding author: Keqiu Li.)
Digital Object Identifier no. 10.1109/TMC.2019.2962129

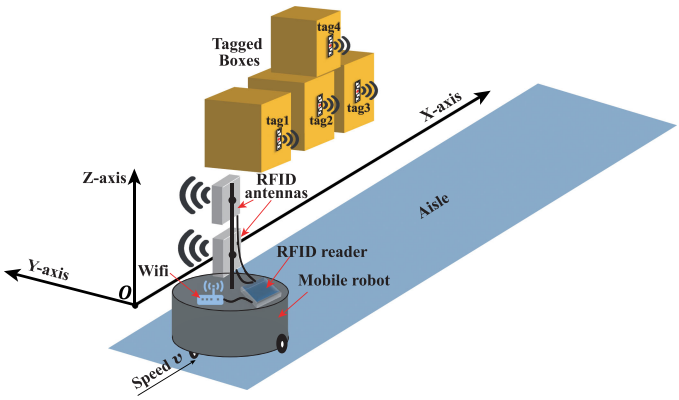

Fig. 1. Illustrating the studied problem: 3D localization of tagged objects using a mobile RF-robot.

antennas. Such kind of systems are hard to be widely applied as it is not easy to buy the these hardware components form general manufactures. *Only 2D localization*: The Spatial-Temporal Phase Profiling (STPP) system [34] and the RF-Scanner [24] system mainly focus on 2D localization problems, but fail in the general application scenarios where 3D localization is desired. *Localization blind zone*: The STPP system needs the robot to pass by the target tag, hence, localization is not achievable if the target object is in a corner. *Low scalability*: The RFID localization systems proposed in [23], [29], [30], [31], [32], [33] need to precisely calibrate the reader antennas at fixed positions. To cover a large region, we have to deploy multiple sets of readers and the involved cost is in proportion to the monitoring area.

1.3 Proposed Localization Approach

To overcome the limitations of existing RFID localization systems, we design and implement a Mobile RF-robot Localization (MRL) system, which is consisted of a backend server, a smart robot (EAI Dashgo D1 [35]), a commodity RFID reader (Impinj R420), and reader antennas (Laird S9028PCL). For easy understanding, we will first discuss 2D localization, i.e., assuming the target tag is on the X–Y plane. Note that, for 2D localization, we only use the below reader antenna, which is also on the X–Y plane. Later, we will explain how to extend it to deal with 3D localization, which requires two reader antennas simultaneously.

The basic principle of the MRL system is as follows. When the robot moves along a straight aisle in a warehouse with a constant speed v, the reader keeps reading the target tag and forwards the received low-level RFID data (e.g., tag ID, phase, antenna port, and timestamp) to the server. Using the tag ID information, we can filter out the irrelevant tag readings. Moreover, we use the antenna port information to know from which antenna a certain tag reading comes. Hence, it is easy to extract the phase profile with timestamps of the target tag corresponding to a certain reader antenna. For 2D localization, we leverage the tag phase profile corresponding to the antenna on X–Y plane. We equally partition the phase profile into three segments and take one phase point from each phase segment. Then, we leverage the spatial and temporal changes hidden in the phase triad to construct an equation set, in which the coordinates of target tag (i.e., x and y) are involved. Solving the equation set, we can achieve the location (x, y) of the target tag. Since there are multiple phase triads in the phase profile, MRL can calculate multiple candidate locations of the target tag. Simply, their average can be reported as the 2D localization result.

1.4 Challenges and Solutions

The first technical challenge is to remove the periodic jump in phase profile, which makes the raw phase profile seemingly messy and hard to understand. Since the distance between target tag and reader antenna changes smoothly, the phase profile reflecting tag-antenna distance is expected to be continuous. However, we always observe periodic jumps in phase profile, i.e., phase value suddenly jumps from around 0 to around 2π or from around 2π to around 0. In this paper, we use the method similar with the `unwrap` command in Matlab [36] to remove the phase jumps in the phase profile by pulsing or minusing multiples of 2π when the absolute phase jumps between consecutive phase values are greater than or equal to the default jump tolerance. The unwrapped phase profile will have no ambiguity in reflecting the changing trend of tag-antenna distance.

The second technical challenge is to theoretically quantify the deviation of each candidate location of target tag. There are multiple phase triads in the phase profile and each of them can be used to calculate a candidate location of the target tag. Although simple, it is far from optimal to use their average as the final tag location because each candidate tag location has a different deviation from the ground truth. Therefore, we propose theoretical analysis to calculate the variance of each candidate tag location. Then, we assign a larger weight to the candidate tag location that has a smaller variance, and vice versa. The weighted average of these candidate tag locations is returned as the final localization result. We find that the weighted average tag location can converge to the ground truth more quickly than the simply averaged result.

The third technical challenge is to extend the MRL system to address the 3D localization problem. At the very beginning, we assume that the target tag is on the X–Y plane and the proposed MRL system can only address the localization problem in 2D plane. To achieve 3D localization, we use two associated reader antennas to read the target tag instead of only using the below antenna. Then, we consider the two intersecting planes in the 3D space. Specifically, the first (second) plane is posed by the tag position and the trajectory of the below (above) antenna. We use the 2D localization approach in Section 1.3 to extract the relative tag locations on each plane. Finally, we use the geometric relationships among target tag and the trajectories of two antennas to extract the tag location in the 3D space.

1.5 Contributions and Advantages Over Prior Work

The key contributions made in this paper are in proposing the MRL system for 3D localization and addressing the three technical challenges. The advantages of the proposed MRL system over the existing RFID localization systems are four-fold. (1) All hardware components of MRL are available in commodity shelfs, hence, it can be easily re-implemented by anyone who requires indoor object localization; (2) MRL is able to enable 3D localization and suitable for more general scenarios; (3) MRL can locate a target tag before passing by it, thus workable for tagged objects in

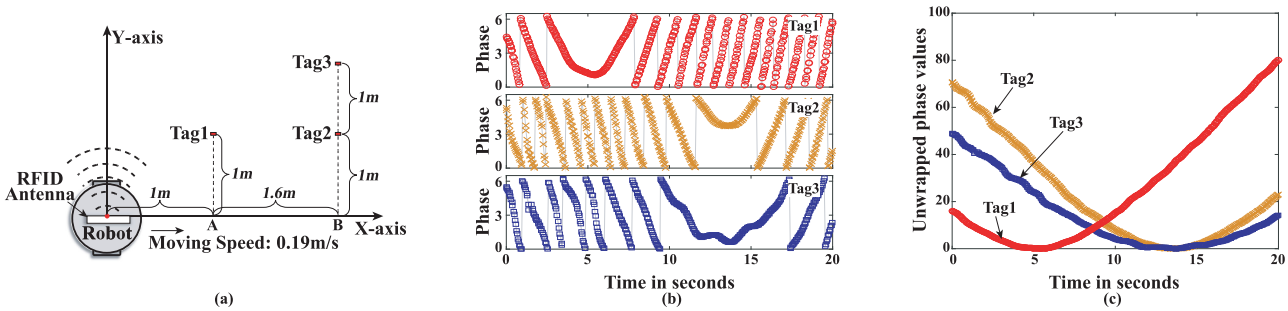

Fig. 2. Processing phase profile. (a) Illustrating the experiment deployment. (b) Raw phase profiles. (c) Unwrapped phase profiles.

corner; (4) Since MRL can locate the target tag in a mobile manner, we only need to deploy a single mobile localization system for a large region. The cost for large-scale scenarios is significantly reduced.

The remainder of this paper is organized as follows. In Section 2, we first present some background knowledge of RFID phase, and then elaborate on removing the periodic jumps in phase profile. In Section 3, we describe the details of our MRL system. In Section 4, we conduct experiments to evaluate the performance of the MRL system in various conditions. We discuss the related work in Section 5. Finally, Section 6 concludes this paper.

2 Understanding and Preprocessing Phase

2.1 Understanding the RFID Phase Profile

We suppose that the RFID reader has received n readings from the target tag with id. Thus, we have n phase points in the raw phase profile: $\mathcal{P}(id,t_1),\mathcal{P}(id,t_2),\ldots,\mathcal{P}(id,t_n)$ while the timestamps $t_1,t_2\ldots t_n$ are in an ascending order, i.e., for any $1\leq i<j\leq n$, we have $t_i<t_j$. We use $dis(id,t_i)$ to denote the distance between the reader antenna and the tag id at time t_i. The signal traverses a total distance of $2\times dis(id,t_i)$ back and forth in backscatter communication. Besides phase rotation over distance, the reader's transmitter circuits, the tag's reflection characteristic, and the reader's receiver circuits will also introduce some additional phase rotations, denoted as θ_T, θ_{TAG} and θ_R respectively [23]. The phase value $\mathcal{P}(id,t_i)$ returned by the RFID reader can be expressed as follows:

$$\mathcal{P}(id,t_i)=\left[\frac{2\times dis(id,t_i)}{\lambda}\times 2\pi+\Theta\right]\bmod 2\pi. \tag{1}$$

Here, λ is the wavelength of the RFID signal, and the constant Θ, called hardware diversity, equals $\theta_T+\theta_{TAG}+\theta_R$.

Next, we conduct a set of experiments to better understand the phase profile. As illustrated in Fig. 2a, we deploy three slim RFID tags vertically in the system. The moving speed v of the robot is set to $0.19m/s$. The RFID reader keeps interrogating tags during the moving process, and the collected raw phase profiles of these three tags are plotted in Fig. 2b, respectively. The raw phase profile of each tag involves the following two types of phase noises. (i) *Random error*: The authors of [23] conducted an empirical study over 100 tags with environment temperature from 0°C to 40°C, and pointed out that phase measurement results inevitably contain random errors, following a typical Gaussian distribution with a standard deviation of 0.1 radians. (ii) *Periodic jump*: according to Eq. (1), the tag phase is a periodic function that repeats if the distance between the reader antenna and tag changes by $\lambda/2$. We first investigate how to remove periodic jumps from the phase profile, and will take random errors into consideration when quantifying the deviation of localization results.

2.2 Eliminating the Periodic Jump

As shown in Fig. 2b, the raw tag phase profile involves periodic phase jumps due to the `mod` operation in Eq. (1). These phase jumps are either from a phase value around 0 to a follow-up phase value around 2π or from a phase value around 2π to a follow-up phase value around 0. We can use a method similar with the `unwrap` command in Matlab [36] to remove the phase jumps in the phase profile $\mathcal{P}(id,t_1),\mathcal{P}(id,t_2),\ldots,\mathcal{P}(id,t_n)$ by pulsing or minusing multiples of 2π when the absolute phase jumps between consecutive phase values are greater than or equal to the default jump tolerance. Using such a method, we can remove the impact of `mod` operation and obtain a new sequence of unwrapped phase values: $\mathcal{P}'(id,t_1),\mathcal{P}'(id,t_2),\ldots,\mathcal{P}'(id,t_n)$, which looks like a shape of V. Specifically, an arbitrary phase point $\mathcal{P}'(id,t_i)$ in the unwrapped phase profile can be expressed as follows:

$$\mathcal{P}'(id,t_i)=\frac{2\times dis(id,t_i)}{\lambda}\times 2\pi+\Theta+2k\pi, \tag{2}$$

where k is a constant integer within $\{0,\pm1,\pm2,\ldots\}$. Next section will use the unwrapped phase profile to calculate tag location.

3 The Proposed MRL System

In this section, we will first describe the Mobile RF-robot Localization (MRL) system for the simple case of 2D localization. After that, we will explain how to extend MRL to enable the 3D localization for general application scenarios.

3.1 Detailed Design of MRL for 2D Localization

For a target tag on the `X-Y` plane, we still suppose the reader has received its n replies. Thus, we have n unwrapped phase points after unwrapping operations: $\mathcal{P}'(id,t_1),\mathcal{P}'(id,t_2),\ldots,\mathcal{P}'(id,t_n)$. The proposed MRL system equally partitions the n unwrapped phase points into three segments: $[\mathcal{P}'(id,t_1),\ldots,\mathcal{P}'(id,t_w)]$, $[\mathcal{P}'(id,t_{w+1}),\ldots,\mathcal{P}'(id,t_{2w})]$, $[\mathcal{P}'(id,t_{2w+1}),\ldots,\mathcal{P}'(id,t_{3w})]$, where $w=\lfloor\frac{n}{3}\rfloor$. Then, we take the ith phase value $\mathcal{P}'(id,t_i)$ from the first segment, the ith phase value $\mathcal{P}'(id,t_{w+i})$ from the second segment, and the

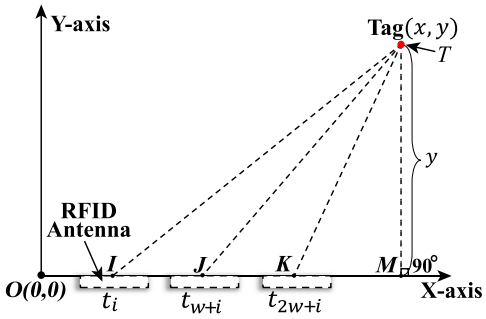

Fig. 3. Exemplifying the principle of the MRL system for 2D localization.

ith phase value $\mathcal{P}'(id, t_{2w+i})$ from the third segment, where $i \in [1, w]$. Next, we will describe how to use these three picked phase values to calculate the location of target tag. Since there are w such phase triads, the MRL system can calculate w candidate tag locations. To distinguish these candidate tag locations from each other, we use (x_i, y_i) to denote the candidate tag location calculated from the phase triad: $\mathcal{P}'(id, t_i)$, $\mathcal{P}'(id, t_{w+i})$, and $\mathcal{P}'(id, t_{2w+i})$. As exemplified in Fig. 3, we assume that the reader antenna arrives at the locations I, J, K at the time points of t_i, t_{w+i}, t_{2w+i}, respectively. According to Eq. (2), we can calculate the difference between adjacent phase points $\mathcal{P}'(id, t_i)$ and $\mathcal{P}'(id, t_{w+i})$, and the difference between adjacent phase points $\mathcal{P}'(id, t_{w+i})$ and $\mathcal{P}'(id, t_{2w+i})$ as follows:

$$\begin{aligned}\mathcal{P}'(id, t_i) - \mathcal{P}'(id, t_{w+i}) &= \frac{4\pi \times \left(|\overrightarrow{IT}| - |\overrightarrow{JT}|\right)}{\lambda} \\ \mathcal{P}'(id, t_{w+i}) - \mathcal{P}'(id, t_{2w+i}) &= \frac{4\pi \times \left(|\overrightarrow{JT}| - |\overrightarrow{KT}|\right)}{\lambda}.\end{aligned} \tag{3}$$

According to the geometric relationships shown in Fig. 3, we also have the following equations:

$$\begin{cases} |\overrightarrow{IT}| = \sqrt{|\overrightarrow{IM}|^2 + |\overrightarrow{MT}|^2} \\ \overrightarrow{IM} = \overrightarrow{IK} + \overrightarrow{KM} \\ |\overrightarrow{JT}| = \sqrt{|\overrightarrow{JM}|^2 + |\overrightarrow{MT}|^2} \\ \overrightarrow{JM} = \overrightarrow{JK} + \overrightarrow{KM} \\ |\overrightarrow{KT}| = \sqrt{|\overrightarrow{KM}|^2 + |\overrightarrow{MT}|^2} \\ \overrightarrow{KM} = \overrightarrow{OM} - \overrightarrow{OK} \\ \overrightarrow{IK} = [v(t_{2w+i} - t_i), 0] \\ \overrightarrow{JK} = [v(t_{2w+i} - t_{w+i}), 0] \\ \overrightarrow{OK} = (vt_{2w+i}, 0) \\ \overrightarrow{MT} = (0, y) \\ \overrightarrow{OM} = (x, 0) \end{cases}.$$

By substituting the above equations into Eq. (3), we obtain an equation set that contains two unknown variables x and y. Then, we solve the equation set to get the candidate tag location (x_i, y_i)

$$\begin{aligned} x_i \leftarrow x &= vt_{2w+i} + \frac{(\frac{\lambda\Delta\theta_2}{4\pi})^2 - v^2\Delta T_2^2 + \frac{\lambda\Delta\theta_2\mathcal{S}}{2\pi}}{2v\Delta T_2}0 \\ y_i \leftarrow y &= \sqrt{\mathcal{S}^2 - (x_i - vt_{2w+i})^2}, \end{aligned} \tag{4}$$

where the values of $\Delta\theta_2$, ΔT_2, and $\mathcal{S}$ are as follows:

$$\begin{cases} \mathcal{S} = \left\{ v^2(\Delta T_1 + \Delta T_2)^2 + \left(\frac{\Delta T_1}{\Delta T_2} + 1\right)\left[\left(\frac{\lambda\Delta\theta_2}{4\pi}\right)^2 - v^2\Delta T_2^2\right] \right. \\ \qquad \left. - \left[\frac{\lambda(\Delta\theta_1 + \Delta\theta_2)}{4\pi}\right]^2 \right\} \Big/ \left(\frac{\lambda\Delta\theta_1}{2\pi} - \frac{\lambda\Delta\theta_2\Delta T_1}{2\pi\Delta T_2}\right) \\ \Delta\theta_1 = \mathcal{P}'(id, t_i) - \mathcal{P}'(id, t_{w+i}) \\ \Delta\theta_2 = \mathcal{P}'(id, t_{w+i}) - \mathcal{P}'(id, t_{2w+i}) \\ \Delta T_1 = t_{w+i} - t_i \\ \Delta T_2 = t_{2w+i} - t_{w+i} \end{cases}.$$

Due to the noise of random errors, the unwrapped phase value has a variance of $Var[\mathcal{P}'(id, t_i)] = 0.01$. Then, the variances of $\Delta\theta_1$ and $\Delta\theta_2$ can be calculated as follows:

$$\begin{aligned} Var(\Delta\theta_1) &= Var[\mathcal{P}'(id, t_i)] + Var[\mathcal{P}'(id, t_{w+i})] = 0.02 \\ Var(\Delta\theta_2) &= Var[\mathcal{P}'(id, t_{w+i})] + Var[\mathcal{P}'(id, t_{2w+i})] = 0.02. \end{aligned}$$

The probabilistic deviation inherent in $\Delta\theta_1$ and $\Delta\theta_2$ also results in that the candidate tag location (x_i, y_i) derived from Eq. (4) is also inaccurate. To quantify the localization deviation, we calculate the variance of x_i and y_i in the following. We observe from Eq. (4) that both x_i and y_i are functions of $\Delta\theta_1$ and $\Delta\theta_2$. Hence, we denote x_i as $\varphi_x(\Delta\theta_1, \Delta\theta_2)$ and y_i as $\varphi_y(\Delta\theta_1, \Delta\theta_2)$, respectively. We present the Taylor's series expansion of x_i and y_i around (h_1, h_2), respectively. Here, $h_1 = E(\Delta\theta_1)$ and $h_2 = E(\Delta\theta_2)$

$$\begin{aligned} x_i &= \varphi_x(h_1, h_2) + \frac{\partial\varphi_x}{\partial\Delta\theta_1}(\Delta\theta_1 - h_1) + \frac{\partial\varphi_x}{\partial\Delta\theta_2}(\Delta\theta_2 - h_2) \\ y_i &= \varphi_y(h_1, h_2) + \frac{\partial\varphi_y}{\partial\Delta\theta_1}(\Delta\theta_1 - h_1) + \frac{\partial\varphi_y}{\partial\Delta\theta_2}(\Delta\theta_2 - h_2). \end{aligned}$$

We have the following equation by taking expectation of both sides of the above two equations, respectively

$$\begin{aligned} E(x_i) &= \varphi_x(h_1, h_2) \\ E(y_i) &= \varphi_y(h_1, h_2). \end{aligned} \tag{5}$$

With Eq. (5), we can calculate the variance of x_i and y_i

$$\begin{aligned} Var(x_i) &= E[x_i - E(x_i)]^2 \\ &= \left(\frac{\partial\varphi_x}{\partial\Delta\theta_1}\right)^2 Var(\Delta\theta_1) + \left(\frac{\partial\varphi_x}{\partial\Delta\theta_2}\right)^2 Var(\Delta\theta_2) \\ Var(y_i) &= E[y_i - E(y_i)]^2 \\ &= \left(\frac{\partial\varphi_y}{\partial\Delta\theta_1}\right)^2 Var(\Delta\theta_1) + \left(\frac{\partial\varphi_y}{\partial\Delta\theta_2}\right)^2 Var(\Delta\theta_2). \end{aligned} \tag{6}$$

As required in Eq. (6), we need to calculate the expressions of $\frac{\partial\varphi_x}{\partial\Delta\theta_1}$, $\frac{\partial\varphi_x}{\partial\Delta\theta_2}$, $\frac{\partial\varphi_y}{\partial\Delta\theta_1}$, and $\frac{\partial\varphi_y}{\partial\Delta\theta_2}$, respectively. Due to the complexity of the expressions, we use some symbols to denote the terms that repetitively appear in equation. Specifically, $\mathcal{A} = v^2(\Delta T_1 + \Delta T_2)^2$, $\mathcal{B} = \frac{\Delta T_1}{\Delta T_2} + 1$, $\mathcal{C} = v\Delta T_2$, $\mathcal{D} = \frac{\lambda\Delta\theta_1}{4\pi}$, $\mathcal{E} = \frac{\lambda\Delta\theta_2}{4\pi}$, $\mathcal{F} = \frac{\lambda(\Delta\theta_1 + \Delta\theta_2)}{4\pi}$. Then, the expressions of $\frac{\partial\varphi_x}{\partial\Delta\theta_1}$ and $\frac{\partial\varphi_x}{\partial\Delta\theta_2}$ are given as follows:

$$\begin{aligned} \frac{\partial\varphi_x}{\partial\Delta\theta_1} &= \frac{-2\mathcal{E}\mathcal{F}(\Delta\theta_1 - (\mathcal{B}-1)\Delta\theta_2) - \Delta\theta_2[\mathcal{A} + \mathcal{B}(\mathcal{E}^2 - \mathcal{C}^2) - \mathcal{F}]}{2\mathcal{C}[\Delta\theta_1 - (\mathcal{B}-1)\Delta\theta_2]^2} \\ \frac{\partial\varphi_x}{\partial\Delta\theta_2} &= \frac{\lambda^2\Delta\theta_2}{\mathcal{C}(4\pi)^2} + \frac{\mathcal{G} - \mathcal{H}}{2\mathcal{C}[\Delta\theta_1 - (B-1)\Delta\theta_2]^2}, \end{aligned} \tag{7}$$

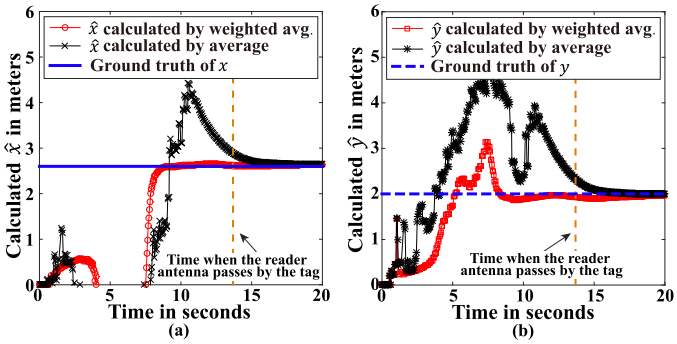

Fig. 4. Comparison between weighted average results and direct average results. (a) Calculated $\hat{x}$ vs. time; (b) Calculated $\hat{y}$ vs. time.

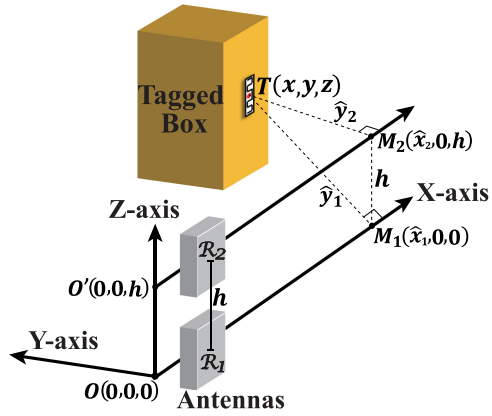

Fig. 5. MRL for 3D localization.

where the expressions of $\mathcal{G}$ and $\mathcal{H}$ are given below:

$$\begin{cases} \mathcal{G} = [\mathcal{A}+\mathcal{B}(\mathcal{E}^2-\mathcal{C}^2)-\mathcal{F}^2+\Delta\theta_2(\frac{2\mathcal{B}\mathcal{E}^2}{\Delta\theta_2}-\frac{\mathcal{F}\lambda}{2\pi})][\Delta\theta_1-(\mathcal{B}-1)\Delta\theta 2] \\ \mathcal{H} = \Delta\theta_2[\mathcal{A}+\mathcal{B}(\mathcal{E}^2-\mathcal{C}^2)-\mathcal{F}^2](1-\mathcal{B}) \end{cases}.$$

And the expressions of $\frac{\partial\varphi_y}{\partial\Delta\theta_1}$ and $\frac{\partial\varphi_y}{\partial\Delta\theta_2}$ are given as follows:

$$\begin{aligned} \frac{\partial\varphi_y}{\partial\Delta\theta_1} &= \frac{2\mathcal{S}\frac{\partial\mathcal{S}}{\partial\Delta\theta_1}-2(x_i-vt_{2w+i})\frac{\partial\varphi_x}{\partial\Delta\theta_1}}{2\sqrt{\mathcal{S}^2-(x_i-vt_{2w+i})^2}} \\ \frac{\partial\varphi_y}{\partial\Delta\theta_2} &= \frac{2\mathcal{S}\frac{\partial\mathcal{S}}{\partial\Delta\theta_2}-2(x_i-vt_{2w+i})\frac{\partial\varphi_x}{\partial\Delta\theta_2}}{2\sqrt{\mathcal{S}^2-(x_i-vt_{2w+i})^2}}, \end{aligned} \tag{8}$$

in which $\frac{\partial\mathcal{S}}{\partial\Delta\theta_1}$ and $\frac{\partial\mathcal{S}}{\partial\Delta\theta_2}$ are calculated as follows:

$$\begin{cases} \frac{\partial\mathcal{S}}{\partial\Delta\theta_1} = \frac{-2\mathcal{F}\lambda[\mathcal{D}-(\mathcal{B}-1)\mathcal{E}]-\lambda\{[\mathcal{A}+\mathcal{B}(\mathcal{E}^2-\mathcal{C}^2)]-\mathcal{F}^2\}}{8\pi[\mathcal{D}-(\mathcal{B}-1)\mathcal{E}]^2} \\ \frac{\partial\mathcal{S}}{\partial\Delta\theta_2} = \frac{2\lambda(\mathcal{B}\mathcal{E}-\mathcal{F})[\mathcal{D}-(\mathcal{B}-1)\mathcal{E}]-\lambda[\mathcal{A}+\mathcal{B}(\mathcal{E}^2-\mathcal{C}^2)-\mathcal{F}^2](1-\mathcal{B})}{8\pi[\mathcal{D}-(\mathcal{B}-1)\mathcal{E}]^2} \end{cases}.$$

So far, we have calculated the candidate location of the target tag, i.e., (x_i, y_i) in Eq. (4), as well as their variances in Eq. (6). Recall that the proposed MRL system can calculate w candidate tag locations: (x_1, y_1), (x_2, y_2) , ..., (x_w, y_w). A straightforward way is to directly use their average as the final localization result. It is simple but far from optimal, because candidate tag locations have different variances. Intuitively, if all three picked phase points lie in the very left part of the unwrapped phase profile (nearly in a straight line), the calculated candidate tag location may be not very accurate. Hence, instead of directly using the average of candidate tag locations, we use their weighted average as the final localization result. A candidate tag location with a smaller variance should be assigned with a larger weight, and vice versa. Hence, we use $\frac{1}{Var(x_i)}$ as the weight of x_i, and use $\frac{1}{Var(y_i)}$ as the weight of y_i. Then, we calculate the final tag location by $\hat{x} = \sum_{i=1}^{w}\frac{x_i}{Var(x_i)\aleph_x}$ and $\hat{y} = \sum_{i=1}^{w}\frac{y_i}{Var(y_i)\aleph_y}$, where $\aleph_x = \sum_{i=1}^{w}\frac{1}{Var(x_i)}$ and $\aleph_y = \sum_{i=1}^{w}\frac{1}{Var(y_i)}$. In Figs. 4a and 4b, we plot the values $\hat{x}$ and $\hat{y}$ that are calculated by the direct average results and the weighted average results, respectively. We make two main observations from the experimental results. First, the weighted average method is faster to converge to the ground truth than the simple average method. Second, the values of $\hat{x}$ and $\hat{y}$ have been already very close to the ground truth at the 7th second, which is 6 seconds earlier than the time when the reader antenna passes by the target tag. Since the robot speed is set to 20 cm/s, it means that MRL can achieve relatively accurate localization result about 1.2 meters before reader antenna passes by the target tag. In other words, the MRL system is able to locate the tagged objects in corner where robot cannot pass by.

3.2 Extending MRL to 3D Localization

The proposed MRL system can be easily extended to enable 3D localization by simultaneously using two reader antennas $\mathcal{R}_1$ and $\mathcal{R}_2$. As illustrated in Fig. 5, we suppose the distance between two reader antennas is h meters. Since the below antenna starts at the point $O(0,0,0)$, the above antenna will start at the point $O'(0,0,h)$. The trajectories of $\mathcal{R}_1$ and $\mathcal{R}_2$ are parallel to each other, and also with a distance of h. As aforementioned, we can leverage the antenna port information in each tag reading to distinguish which antenna the current tag reading is received from. Thus, we can have two phase profiles of the target tag corresponding to these two reader antennas, respectively.

As illustrated in Fig. 5, we have two planes in the 3D space: TOM_1 and $TO'M_2$. On the plane TOM_1, the 2D localization approach described in the above is applied on the phase profile corresponding to antenna $\mathcal{R}_1$ and we can calculate a tag location $(\hat{x}_1, \hat{y}_1)$. We draw a line from tag location $T(x, y, z)$ perpendicularly to the trajectory of $\mathcal{R}_1$, with foot M_1. On the plane of TOM_1, it is easy to know that $|\overrightarrow{OM_1}| = \hat{x}_1$ and $|\overrightarrow{TM_1}| = \hat{y}_1$. Similarly, applying the 2D localization approach on the phase profile from $\mathcal{R}_2$, MRL can also calculate a tag location $(\hat{x}_2, \hat{y}_2)$, which satisfy that $|\overrightarrow{O'M_2}| = \hat{x}_2$ and $|\overrightarrow{TM_2}| = \hat{y}_2$. It is easy to know that the coordinates of M_1 and M_2 are $(\hat{x}_1, 0, 0)$ and $(\hat{x}_2, 0, h)$, respectively. In the ideal case, we should have $x = \hat{x}_1 = \hat{x}_2$. Due to the deviation in localization results, $\hat{x}_1$ may not exactly equal $\hat{x}_2$. Then, we calculate the coordinate value $x = \frac{\hat{x}_1+\hat{x}_2}{2}$. Next, we investigate how to calculate the coordinate values y and z of the target tag. Three types of geometric relationships in the triangle ΔTM_1M_2 are illustrated in Fig. 6, which correspond to $z \in (0, h]$, $z \leq 0$, $z > h$, respectively. No matter which geometric relationship actually applies, we always have the following equation set:

$$\begin{cases} |\overrightarrow{TM_1}| = \sqrt{y^2+z^2} = \hat{y}_1 \\ |\overrightarrow{TM_2}| = \sqrt{y^2+(z-h)^2} = \hat{y}_2 \end{cases}.$$

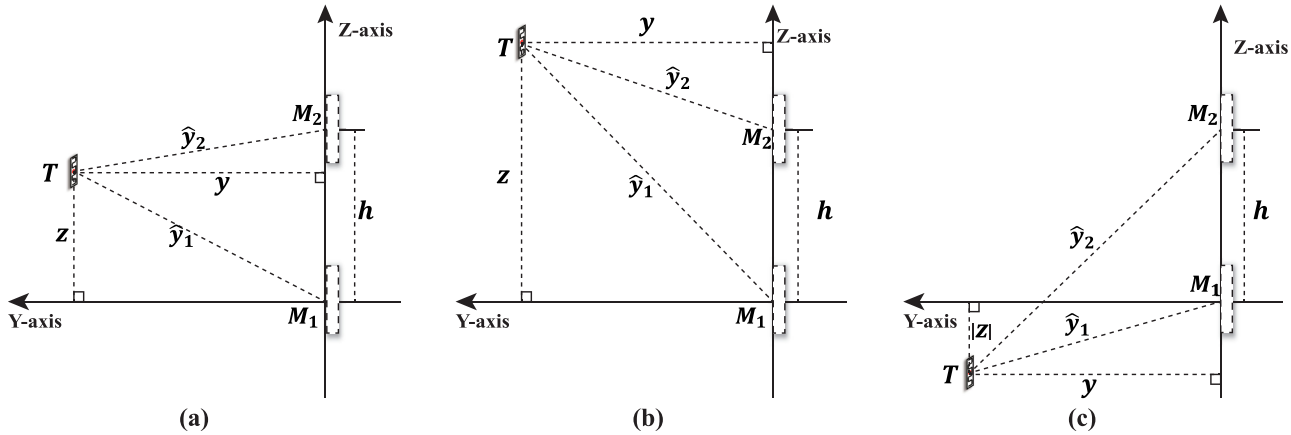

Fig. 6. Geometric relationship between variables y, z, $\hat{y}_1$, $\hat{y}_2$, and h. (a) $0 < z \leq h$. (b) $z > h$. (c) $z \leq 0$.

By solving the above equation set, we can calculate the coordinates of the target tag in 3D space as follows:

$$\begin{cases} \hat{x} = \frac{\hat{x}_1+\hat{x}_2}{2} \\ \hat{y} = \sqrt{(\hat{y}_1)^2 - [\frac{(\hat{y}_1)^2-(\hat{y}_2)^2+h^2}{2h}]^2}\,. \\ \hat{z} = \frac{(\hat{y}_1)^2-(\hat{y}_2)^2+h^2}{2h} \end{cases}$$

So far, the MRL system has been extended to successfully enable the 3D localization functionality.

3.3 Phase Unwrapping Error and Solution

Due to physical thrill of the mobile robot itself or environmental interference, the phase data collected by RFID reader

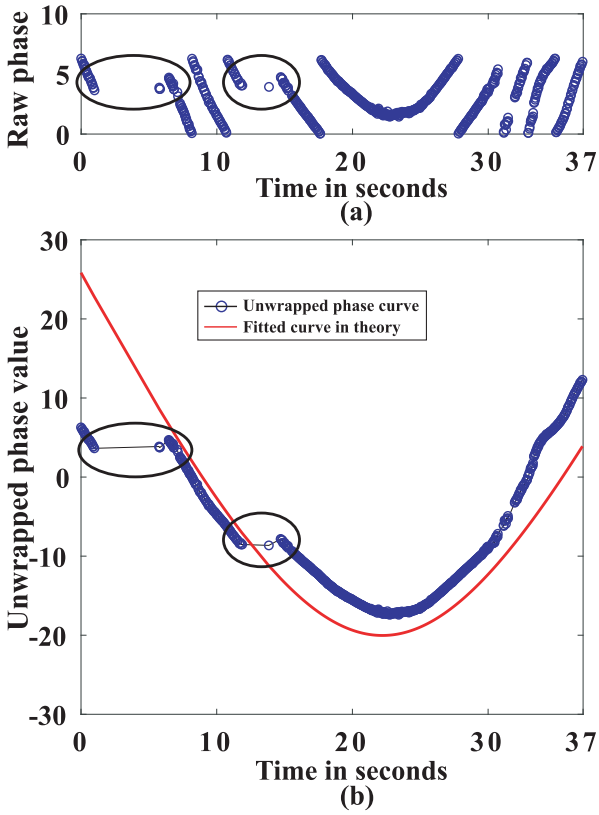

Fig. 7. Exemplifying the phase unwrapping error. (a) Raw phase data. (b) Unwrapped phase data and fitted curve.

are not always perfect and we may not correctly perform the unwrapping operations. As exemplified in Fig. 7, there are two notable time gaps (marked by the circles) in the raw phase profile. In the corresponding experiments, the ground truth of x and y is $2.14m$ and $0.77m$, respectively. The robot moving speed is set to 9.4 cm/s. Using the unwrapping method in [24], we will get an incorrect unwrapping phase profile. Applying the hyperbola fitting algorithm [24] on such an unwrapping phase profile, the localization result is $(2.09m, 1.24m)$, where the value $\hat{x}$ is very close to the ground truth while $\hat{y}$ is clearly over calculated. The following method is proposed to alleviate the side effect of such phase unwrapping error. In MRL, we find the large gaps in the phase profile that are larger than a given threshold and then divide the whole phase profile into multiple phase segments. Note that, the threshold is set to $10 \times \frac{\texttt{Time duration}}{\#\ \texttt{oftag reading}}$ throughout this paper. We should guarantee that, in each segment, the gap between any two adjacent phase points is less than the given threshold. Then, we apply the aforementioned MRL algorithm on each phase segment and get a corresponding localization result. We eventually output the average of these localization results. Applying this method on the phase data of Fig. 7, we find that the localization result of the MRL system is very close to the ground truth.

4 Performance Evaluation

In this section, we first specify the details about system implementation from the perspectives of hardware components and software configuration. After that, we describe the experimental conditions that we employ by default. Finally, we conduct extensive experiments to evaluate the performance of the MRL system.

4.1 Implementation Details

4.1.1 Hardware Components

As illustrated in Fig. 8, the proposed MRL system consists of the following hardware components: a Thinkpad Carbon X1 desktop, an EAI Dashgo D1 smart robot, an Impinj R420 reader, two Laird S9028PCL reader antennas, and several impinj e41c tags. RFID reader works at the UHF band 902~928 MHz. To eliminate the channel hopping issue, we fix the working frequency at 920.625 MHz. We configure the reader transmission

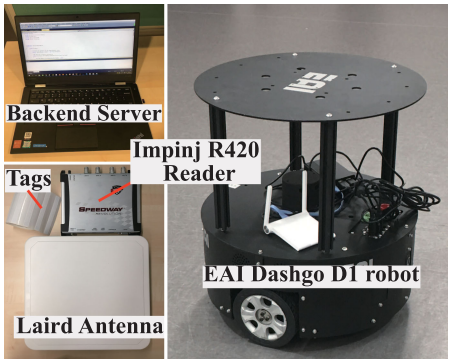

Fig. 8. The hardware components of the proposed MRL system.

power to 32.5 dBm. Generally, the RFID systems use either linear antennas or circular polarization antennas [37]. Compared with the circular polarized antennas of the same gain, the linear polarized antennas normally have a bit longer read range. However, the linear antennas require that tags under interrogation has to be in a polarization matching condition with the reader antenna. However, this cannot be predictable in the warehouse scenario. Hence, we use the circular polarization antennas in this paper. The circularly polarized Laird S9028PCL antenna is of the gain 8.5 dBic and also operates within 902∼928 MHz. The RFID reader reports the low level RFID data to the desktop via a WiFi embedded in the robot.

4.1.2 Software Configuration

The robot is controlled by an arduino board with a bluetooth communication module. Utilizing the Bluetooth channel, we have an application on the smart phone to control the robot movement with given direction and speed. On the server side, we first adopt the LLRP protocol [38], which is implemented in Java, to configure the reader to read the low level RFID data (e.g., tag ID, phase, timestamp) from tags. The collected RFID data are timely stored in a local file on the server. At the same time, MRL reads the data from this local file to calculate the tag location.

4.2 Experiment Conditions

The material of the tagged objects is an important factor that may significantly affect the performance of the localization algorithms [39]. For example, if we directly attach a tag on a metal plate or a water bottle, RFID reader even cannot read the tag at all. Hence, without otherwise specified, we will attach RFID tags on the cartons (made of paperboard) by default. On the other hand, the indoor environment may also significantly affect the localization result, because multi-path caused by walls, apparatus and moving human beings makes the signal propagation unstable [40]. Following the experiment settings of the state-of-the-art RF-Scanner localization system [24], we also assume that there is a line-of-sight between reader antenna and tag. In this paper, we use the ALIEN 9,640 tags, which are in the shape of strip. Moreover, the tags are placed vertically as default, i.e., the tag orientation is along the $\mathtt{Z}-$axis.

4.3 Performance of MRL in 2D Localization

4.3.1 Localization of Multiple Tags

In this set of experiments, we investigate the localization accuracy of the MRL system in the 2D plane. As illustrated

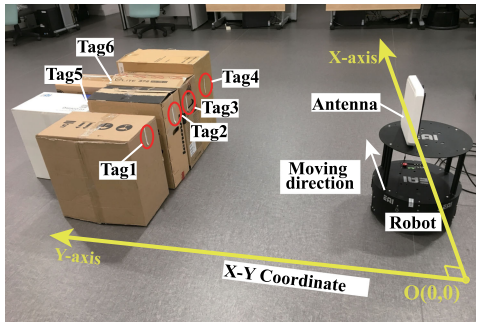

Fig. 9. Deployment of the MRL system in the 2D plane.

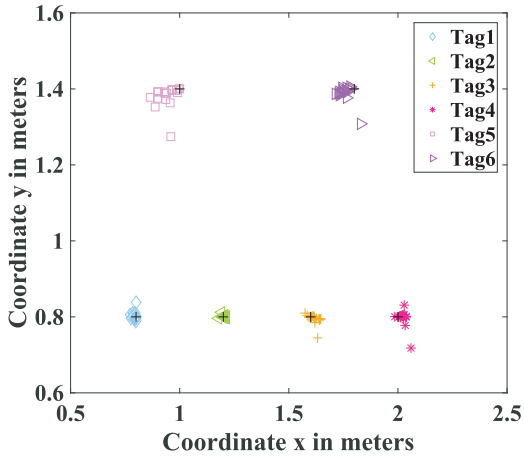

Fig. 10. Localization results of multiple RFID tags in 2D plane.

in Fig. 9, we attach 6 tags to 6 cartons. The tagged cartons are placed more than $0.8m$ away from the trajectory of the moving robot. The actual tag locations are marked by "+" in Fig. 10. The reader antenna and these 6 tags are on the same plane. The MRL system passes by these tagged cartons with a speed $v = 0.1$ m/s and then reports their locations. The same experiment is repeated for several times, and the localization results are also plotted in Fig. 10. We observe that the calculated locations for each tag are very close to the ground truth. For a tag with location (x, y), if the calculated location is $(\hat{x}, \hat{y})$, we refer to $|x - \hat{x}|$ as the localization error in $\hat{x}$, and similarly refer to $|y - \hat{y}|$ as the localization error in $\hat{y}$. For clearly evaluating the localization accuracy of MRL, we also plot the CDF curves of localization errors in $\hat{x}$ and $\hat{y}$ in Fig. 11. We observe from Fig. 11 that, the localization errors along $\mathtt{X}-$axis are generally less than that along $\mathtt{Y}-$axis. The results in Figs. 11a, 11b, 11c, and 11d reveal that localization errors of the MRL system are less than 5 cm with a probability larger than 90 percent. However, localization errors of Tag 5 and Tag 6 are a bit larger than that of the other tags, because signals of these two tags are affected by the cartons in the line-of-sight path to the reader antenna.

4.3.2 Impact of Tag Coupling

In this set of experiments, we investigate whether the interference from nearby tags could affect the phase profile of the target tag. First, we conduct an experiment to show and explain the interference of nearby tags. Specifically, we fix a tag in front of the reader antenna, and then move another tag gradually closer to the fixed tag. Since the distance between the fixed

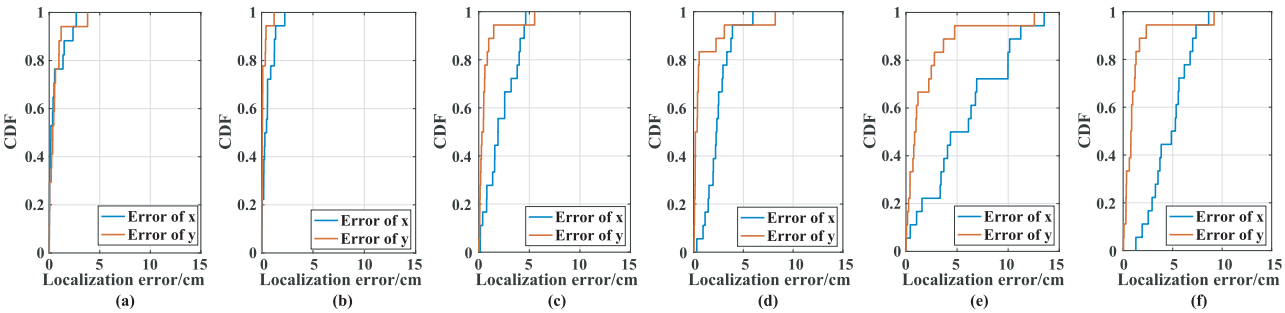

Fig. 11. CDF of localization errors of the proposed MRL system in 2D plane. (a) Tag 1. (b) Tag 2. (c) Tag 3. (d) Tag 4. (e) Tag 5. (f) Tag 6.

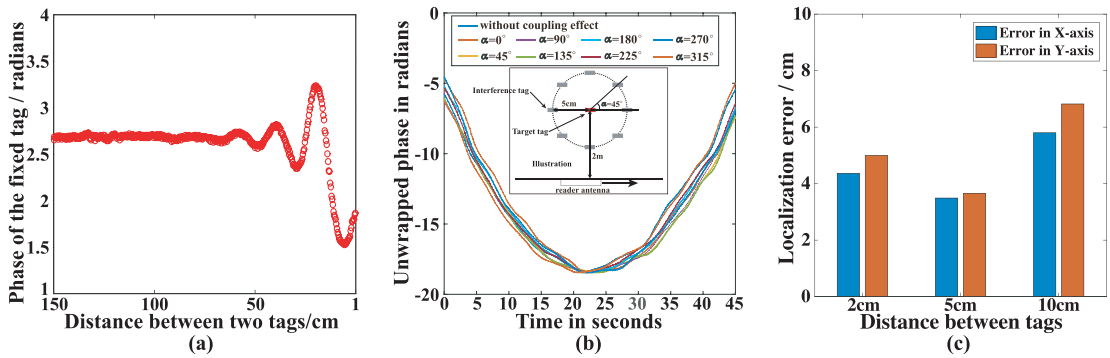

Fig. 12. Investigating the impact of coupling effect. (a) Verifying the existence of coupling effect. (b) Comparing unwrapped phase profiles with and without coupling effect. (c) Investigating the impact of tag coupling effect on localization accuracy of MRL.

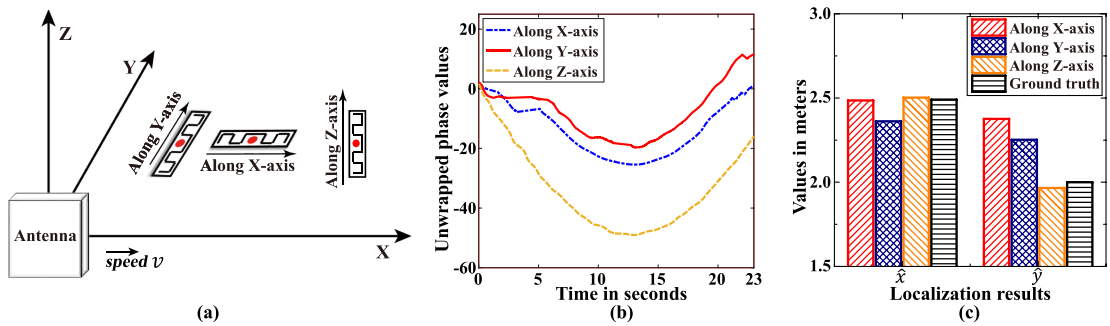

Fig. 13. Investigating the impact of tag orientation on the MRL approach. (a) Illustrating the placement of reader antenna and tags. (b) Comparing the unwrapped phase values of different tag orientation. (c) Comparing the localization results corresponding to different tag orientation.

tag and the reader antenna does not change over time, the phase value of the fixed tag is expected to remain stable in theory. However, the experimental results in Fig. 12a reveal that the phase value of the fixed tag is seriously affected when the distance between these two tags is smaller than 50 cm. Such a phenomenon is caused by the coupling effect [41]. A natural question is: does the MRL system still work well in the practical RFID systems that are full of coupling effect caused by adjacent tags? To investigate the impact of tag coupling effects on the MRL system, we did the following experiments. We first put the target tag at a fixed location, and use the moving antenna to collect its phase profile. After that, we place another tag d centimeters away from the target tag in different directions (the angle α illustrated in Fig. 12b varies from 0 to 315 degree), thereby deliberately causing coupling effect. For a specific α, we use the moving antenna to collect the phase profile of the target tag again. The unwrapped phase profiles with and without coupling effect are plotted in Fig. 12b. Generally, the trend of a phase profile determines the coordinates (x, y) of a tag location, because the MRL system uses the phase difference instead of the absolute phase value. We find that, after aligning these unwrapped phase curves at the bottom (just involving vertical shift), they match well: changing trends of phase profiles are quite similar, and timestamps of bottom points are also almost the same. Hence, we believe the proposed MRL system is immune to the coupling effect. To verify this point, we conduct a new set of experiments to evaluate the localization performance of our MRL system with tag coupling effects. In the experiments, we deployed the target tag at position (1,1). Then, we put an interference tag along the angle $\alpha = 0^\circ$ and vary the distance between target/interference tags from 2 cm to 5 cm and 10 cm. With each tag distance, we use the MRL system to pinpoint the location of target tag. The experimental results in Fig. 12c reveal that tag coupling effects do not affect the performance of the MRL system very much. Note that, the same as the other RFID localization systems, the localization accuracy of MRL is highly affected by the environmental factors. Although we repeat

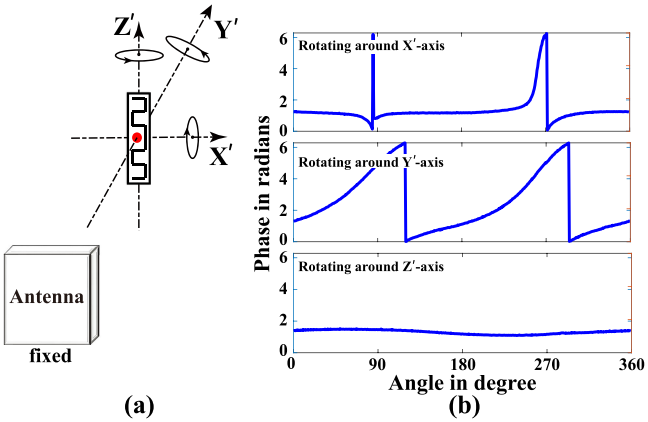

Fig. 14. Measuring phase values of a tag with different rotation angles. (a) Rotation mode of the tag. (b) Phase values vs. rotation angle.

each set of experiments for multiple times and report the average results, the localization results are still not always stable.

4.3.3 Impact of Tag Orientation

Here, we desire to investigate the impact of tag orientation on the localization accuracy of the proposed MRL system. Hence, we place a tag at the same location but along three representative directions sequentially. The tag orientations along X-axis, Y-axis, and Z-axis are illustrated in Fig. 13a, respectively. For each type of tag placement, we run the MRL system to calculate the location of this tag. After performing these three experiments, we plot the corresponding unwrapped phase curves in Fig. 13b. Moreover, the localization results corresponding to these tree experiments are plotted in Fig. 13c. It is easy to observe that, the localization results are much more close the ground truth when the tag orientation is along Z-axis, i.e., vertically placing the tag. Hence, we can assert that tag orientation indeed affects the localization accuracy. To explore the underlying reasons, we place a tag at a fixed location as illustrated in Fig. 14a, and construct another coordinate system for it, i.e., X'-axis is the parallel to the long side of this tag; Y'-axis is perpendicular to the tag plane; and Z'-axis is the parallel to the short side of this tag. Then, we rotate the tag around different axes, respectively, meanwhile, the reader keeps interrogating the tag and records the phase values. Note that, Wei *et al*. conducted experiments to investigate the impact of tag orientation on phase [41]. To be self-contained, we conduct similar experiments and plot the results in Fig. 14b, i.e., showing tag phase values with respect to different rotation angles. We observe that, the phase values are not stable when the tag rotates around X'-axis and around Y'-axis. This phenomenon is caused by the polarity of RFID reader antennas [41]. On the contrary, the phase values are stable when the tag rotates around Z'-axis. Getting back to the experiments corresponding to Fig. 13, if the target tag is placed along X-axis, the movement of the reader antenna causes the relative tag rotation around the X'-axis of this tag, which results in instable phase values and further poor localization accuracy as well. The poor localization accuracy when tag is placed along Y-axis can be explained by similar reasons. Due to the great localization accuracy when tag is placed along Z-axis, we suggest placing the tag vertically in practice, e.g., tags are vertically placed in book spine.

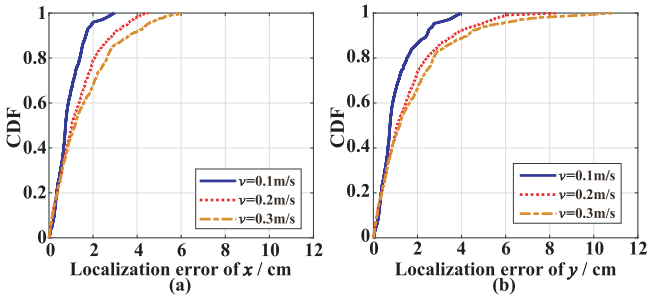

Fig. 15. Localization errors vs. different robot moving speeds. (a) CDF of localization errors in $\hat{x}$. (b) CDF of localization errors in $\hat{y}$.

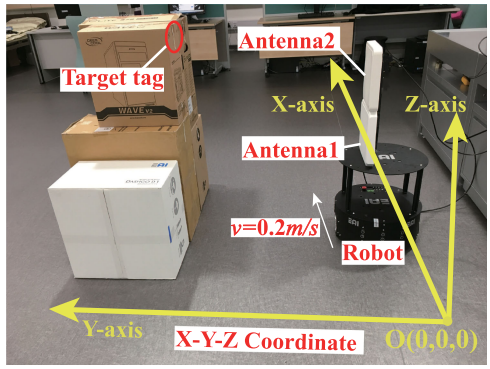

Fig. 16. Deployment of the MRL system in the 3D space.

4.3.4 Impact of Moving Speed

In this set of experiments, we investigate the impact of moving speed on the localization accuracy of our MRL system. The target tag is placed at the location $(2m, 2m)$ in the 2D plane. We vary the speed of the MRL system from 0.1 m/s to 0.3 m/s. The CDF curves of localization errors in $\hat{x}$ and $\hat{y}$ with different speeds are plotted in Figs. 15a and 15b, respectively. We observe that, as the speed increases, the localization errors will also increase accordingly. The possible reasons behind this observation are as follows. First, the higher the moving speed is, the more sparse the phase profile will be, which will further deteriorate the localization accuracy. Second, the higher moving speed of the robot will cause more mechanical jitter. Therefore, the tag phase value, which highly depends on the distance between the reader antenna and target tag, is also unstable.

4.4 Performance in 3D Localization

4.4.1 Localization Accuracy Versus Tag Positions

As illustrated in Fig. 16, we fix two antennas with a distance $h = 0.7m$ meters on the robot. The moving trajectory of antenna $\mathcal{R}_1$ is treated as the positive direction of the X-axis. In such a coordinate system, we place a target tag at different positions. The ground truth of x varies from $1m$ to $1.5m$; the ground truth of y varies from $0.6m$ to $0.8m$ and $1m$; the ground truth of z varies from $0.35m$ to $0.7m$. The MRL system moves with a speed of 10 cm/s and pinpoints the tag location. The experimental results shown in Fig. 17 reveal the 3D localization accuracy of the proposed MRL system: most localization errors along the X− and Y−axes are less than $7cm$ and most localization errors along the Z−axis are less than $12cm$. Such a localization accuracy can satisfy the requirements of most application scenarios.

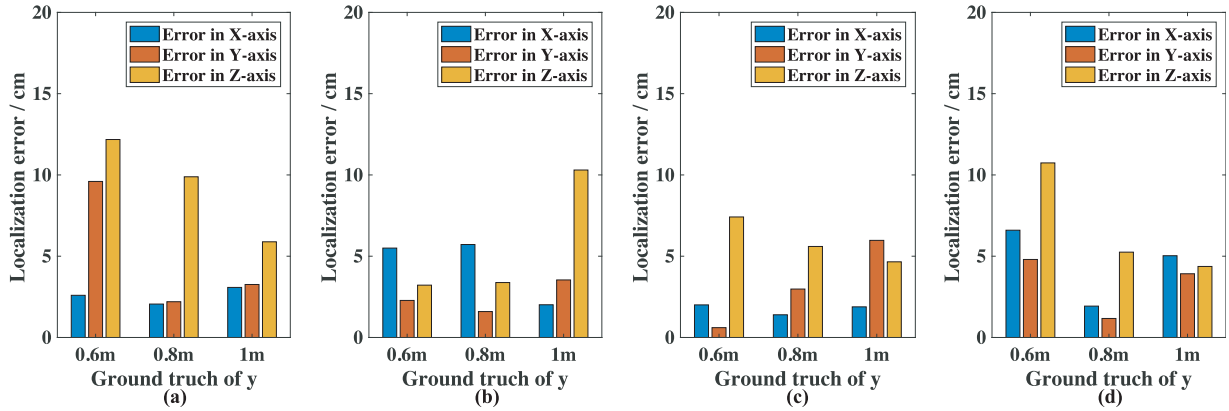

Fig. 17. Investigating localization accuracy of MRL vs. different tag positions. (a) tag is placed at $(1m, y, 0.35m)$. (b) tag is placed at $(1.5m, y, 0.35m)$. (c) tag is placed at $(1m, y, 0.7m)$. (d) tag is placed at $(1.5m, y, 0.7m)$. y varies from $0.6m$ to $0.8m$ and $1m$.

4.4.2 Localization Accuracy Versus Antenna Distance

In this set of experiments, we place a target tag at the fixed location $(1m, 1m, 0.35m)$ in the 3D space and vary the distance between two reader antennas from 30 cm to 50 cm and $70cm$ in each localization process. The experimental results shown in Fig. 18 reveal that, the reader antenna distance does not affect the localization errors in X−axis very much. On the contrary, a large antenna distance will generally reduce the localization errors in Y− and Z−axes. We will elaborate on the impact of h on the localization errors. According to the analysis in Section 3.2, the value z is calculated by $\hat{z} = \frac{(\hat{y}_1)^2 - (\hat{y}_2)^2 + h^2}{2h}$. And it is easy to have that the actual value z satisfies $z = \frac{(y_1)^2 - (y_2)^2 + h^2}{2h}$. Next, we calculate the localization error in z as $|z - \hat{z}| = \frac{[(y_1)^2 - (\hat{y}_1)^2] - [(y_2)^2 - (\hat{y}_2)^2]}{2h}$. For the same pair of calculated values $\hat{y}_1$ and $\hat{y}_2$, the localization error in z is significantly affected by the distance h between two reader antennas. A larger antenna distance h will generally result in a smaller localization error in Z−axis. Similar reasons can explain the impact of h on the localization error in Y−axis.

5 Related Work

We summarize and divide the existing RFID localization approaches into the following two categories.

RSS-Based Approaches. The pioneer localization system, e.g., LANDMARC [29], is based on RSS. It requires to deploy dense reference tags in the surveillance region in advance. An insight is that, the nearby tags have similar distance from the RFID reader antenna. Hence, their RSS values should also be similar. Then, LANDMARC finds out k reference tags whose RSS values are the most similar with the target tag, and uses the weighted average of these k reference tags' locations as the localization result. BFVP [42] approach consists of two stages, i.e., an observation collecting stage and a tag location estimating stage. In the first stage, the robot carrying RFID reader antennas stops at several locations in the given region. At each stop, the RFID reader uses different RF transmission power to scan tags, and a vector is created to present whether the target tag is read or not at every RF power. In the second stage, a Bayesian filter approach using a varying power RFID model is deployed to calculate the location of the target tag based on its all collected vectors. BFVP highly relies on the RFID power model, which is developed through experiments. The developed model cannot be seamlessly adopted by a new application scenario due to different environmental factors such as obstacles, materials, and multi-path.

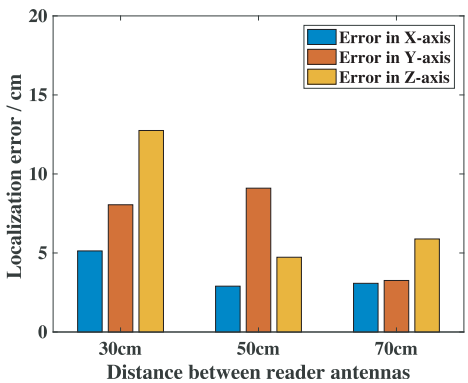

Fig. 18. Investigating the localization accuracy of the MRL system with different distances between reader antennas.

Phase-Based Approaches. In recent years, we have witnessed a growing interest in using RF phase information to address the RFID localization problem. The Angle of Arrival (AoA) based localization algorithms use multiple reader antenna arrays. In each array, they use the phase difference to calculate the angle between the target tag and the antenna array plane. With two antenna arrays, they draw two lines according to the measured angles, and the intersection point should be the location of target tag. PinIt [32] uses a moving antenna to measure the multi-path profiles of the reference tags at known positions and locates the target tag according to the insight that adjacent tags have similar multi-path effects. This approach is not easy to use for the anonymous RFID system, where we may know nothing about the reference tags. On the other hand, the complex application scenarios may cause that nearby tags have totally different multi-path effects. DHA [23] partitions the surveillance area into small grids, and uses the phase data collected from the target tag to calculate the probability that this target tag lies in each grid. The grid having the highest probability will be returned as the target tag location. DHA needs sophisticated calibration of multiple reader antennas, which is significantly laborious. Moreover, for applying in a large-scale surveillance region, DHA has to deploy a large number of readers and antennas as well, which will cost a lot. The basic idea of STPP [34] is to use the minimum point of the unwrapped phase profile, which theoretically corresponds to

the time point when the tag is exactly perpendicular to the reader antenna's trajectory, to recognize the order of tags along X–axis. Intuitively, we can also use a slightly modified method to calculate the value x of the target tag location. However, the STPP scheme cannot tell us the value y of the target tag location. The RF-Scanner system [24] was proposed to pinpoint the misplaced books on the shelf. In fact, the localization algorithm used in RF-Scanner only deals with the 2D localization. The calculated coordinate x can be used to pinpoint the order of books in a layer. And the calculated coordinate y can be used to determine which layer a tagged book lies in. For example, if the coordinate y of a book is much larger than a normal value, this book must lie in the upper/lower layer rather than the layer that reader antenna is scanning. However, the RF-Scanner system cannot address the general 3D localization problem studied in this paper. In [43], Emidio DiGiampaolo *et al*. proposed to sue a robot equipped RFID to locate objects on shelves. The localization system involves two steps. First, a Kalman-based algorithm is applied on the RFID phase data collected from the reference tags on shelf to locate the robot itself. Second, they proposed an algorithm to match the phase data collected from the tagged objects on shelf to a parametric model, thereby estimating the position of the objects on the shelf.

6 Conclusion

In this paper, we used COTS robot and RFID devices to implement the Mobile RF-robot Localization (MRL) system, which makes use of spatial and temporal information in the RFID phase profile to accurately locate tags. MRL has four major advantages over the existing RFID localization systems. First, MRL only consists of the COTS devices rather than any specialized devices. Hence, it is easy to be re-implemented for widespread application. Second, MRL is able to address 3D localization and suitable for more application scenarios. Third, MRL can locate tagged objects before passing them, thus does not suffer the limitation of blind zone. Fourth, a single set of MRL system can provide the localization service for a large surveillance region in a mobile manner. Hence, it is cost-efficient for large-scale scenarios. Owing to the above attractive properties, the proposed MRL system has promising prospect in future warehousing and logistics scenarios.

Acknowledgments

This work was supported in part by National Key R&D Program of China under Grant 2019YFB2102404, in part by NSFC under Grant 61772251, in part by Hong Kong RGC Research Impact Fund under Grant R5034-18, in part by Shenzhen Basic Research Funding Scheme under Grant JCYJ20170818104222072, in part by the National Science Foundation under Grant Number CNS-1837146, in part by a Canada NSERC Discovery Grant, in part by Technology Demonstration Program (TDP) Grant, in part by Key Research and Development Program for Guangdong Province under Grant No. 2019B010136001, in part by the Science Innovation Foundation of Dalian under Grant 2019J12GX037.

References

[1] A. W. Weiser, Y. Orchan, R. Nathan, M. Charter, A. J. Weiss, and S. Toledo, "Characterizing the accuracy of a self-synchronized reverse-GPS wildlife localization system," in *Proc. 15th ACM/IEEE Int. Conf. Inf. Process. Sens. Netw.*, 2016, pp. 1–12.

[2] Y. Zhang, W. Liu, Y. Fang, and D. Wu, "Secure localization and authentication in ultra-wideband sensor networks," *IEEE J. Sel. Areas Commun.*, vol. 24, no. 4, pp. 829–835, Apr. 2006.

[3] X. Cheng, A. Thaeler, G. Xue, and D. Chen, "TPS: A time-based positioning scheme for outdoor wireless sensor networks," in *Proc. IEEE INFOCOM*, 2004, pp. 2685–2696.

[4] X. Liu, S. Zhang, B. Xiao, and K. Bu, "Flexible and time-efficient Tag Scanning with handheld readers," *IEEE Trans. Mobile Comput.*, vol. 15, no. 4, pp. 840–852, Apr. 2016.

[5] X. Liu, Q. Yang, J. Luo, B. Ding, and S. Zhang, "An energy-aware offloading framework for edge-augmented mobile RFID systems," *IEEE Internet Things J.*, vol. 6, no. 3, pp. 3994–4004, Jun. 2019.

[6] K. Xie *et al.*, "Recover corrupted data in sensor networks: A matrix completion solution," *IEEE Trans. Mobile Comput.*, vol. 16, no. 5, pp. 1434–1448, May 2017.

[7] K. Xie, L. Wang, X. Wang, G. Xie, and J. Wen, "Low cost and high accuracy data gathering in WSNs with matrix completion," *IEEE Trans. Mobile Comput.*, vol. 17, no. 7, pp. 1595–1608, Jul. 2018.

[8] P. Lazik, N. Rajagopal, O. Shih, B. Sinopoli, and A. Rowe, "ALPS: A bluetooth and ultrasound platform for mapping and localization," in *Proc. 13th ACM Conf. Embedded Netw. Sens. Syst.*, 2015, pp. 73–84.

[9] H. Li, L. Sun, H. Zhu, X. Lu, and X. Cheng, "Achieving privacy preservation in WiFi fingerprint-based localization," in *Proc. IEEE INFOCOM*, 2014, pp. 2337–2345.

[10] Y. Wen, X. Tian, X. Wang, and S. Lu, "Fundamental limits of RSS fingerprinting based indoor localization," in *Proc. IEEE INFOCOM*, 2015, pp. 2479–2487.

[11] X. Xiong, Z. Yang, L. Shangguan, Y. Fei, M. Stojmenovic, and Y. Liu, "SmartGuide: Towards single-image building localization with smartphone," in *Proc. 16th ACM Int. Symp. Mobile Ad Hoc Netw. Comput.*, 2015, pp. 117–126.

[12] J. Yu, W. Gong, J. Liu, L. Chen, and K. Wang, "On efficient tree-based tag search in large-scale RFID systems," *IEEE/ACM Trans. Netw.*, vol. 27, no. 1, pp. 42–55, Feb. 2019.

[13] J. Yu, W. Gong, J. Liu, L. Chen, K. Wang, and R. Zhang, "Missing tag identification in COTS RFID systems: Bridging the gap between theory and practice," *IEEE Trans. Mobile Comput.*, vol. 19, no. 1, pp. 130–141, Jan. 2020.

[14] X. Liu *et al.*, "Fast identification of blocked RFID tags," *IEEE Trans. Mobile Comput.*, vol. 17, no. 9, pp. 2041–2054, Sep. 2018.

[15] X. Liu *et al.*, "Fast RFID sensory data collection: Trade-off between computation and communication costs," *IEEE/ACM Trans. Netw.*, vol. 27, no. 3, pp. 1179–1191, Jun. 2019.

[16] X. Liu *et al.*, "Efficient range queries for large-scale sensor-augmented RFID systems," *IEEE/ACM Trans. Netw.*, vol. 27, no. 5, pp. 1873–1886, Oct. 2019.

[17] H. Ding *et al.*, "Trio: Utilizing tag interference for refined localization of passive RFID," in *Proc. IEEE INFOCOM*, 2018, pp. 828–836.

[18] L. Xie, H. Han, Q. Li, J. Wu, and S. Lu, "Efficient protocols for collecting histograms in large-scale RFID systems," *IEEE Trans. Parallel Distrib. Syst.*, vol. 26, no. 9, pp. 2421–2433, Sep. 2015.

[19] Y. Zheng and M. Li, "Fast tag searching protocol for large-scale RFID systems," *IEEE/ACM Trans. Netw.*, vol. 21, no. 3, pp. 924–934, Jun. 2013.

[20] Y. Zheng and M. Li, "ZOE: Fast cardinality estimation for large-scale RFID systems," in *Proc. IEEE INFOCOM*, 2013, pp. 908–916.

[21] S. Chen, M. Zhang, and B. Xiao, "Efficient information collection protocols for sensor-augmented RFID networks," in *Proc. IEEE INFOCOM*, 2011, pp. 3101–3109.

[22] Y. Qiao, S. Chen, T. Li, and S. Chen, "Tag-ordering polling protocols in RFID systems," *IEEE/ACM Trans. Netw.*, vol. 24, no. 3, pp. 1548–1561, Jun. 2016.

[23] L. Yang, Y. Chen, X.-Y. Li, C. Xiao, M. Li, and Y. Liu, "Tagoram: Real-time tracking of mobile RFID tags to high precision using COTS devices," in *Proc. 20th ACM Annu. Int. Conf. Mobile Comput. Netw.*, 2014, pp. 237–248.

[24] J. Liu, F. Zhu, Y. Wang, X. Wang, Q. Pan, and L. Chen, "RF-scanner: Shelf scanning with robot-assisted RFID systems," in *Proc. IEEE INFOCOM*, 2017, pp. 1–9.

[25] H. Ding *et al.*, "RFIPad: Enabling cost-efficient and device-free in-air handwriting using passive tags," in *Proc. IEEE 37th Int. Conf. Distrib. Comput. Syst.*, 2017, pp. 447–457.

[26] L. Xie, J. Sun, Q. Cai, C. Wang, J. Wu, and S. Lu, "Tell me what I see: Recognize RFID tagged objects in augmented reality systems," in *Proc. ACM Int. Joint Conf. Pervasive Ubiquitous Comput.*, 2016, pp. 916–927.

[27] C. Duan, L. Yang, H. Jia, Q. Lin, Y. Liu, and L. Xie, "Robust spinning sensing with dual-RFID-tags in noisy settings," in *Proc. IEEE INFOCOM*, 2018, pp. 855–863.

[28] L. Shangguan, Z. Zhou, X. Zheng, L. Yang, Y. Liu, and J. Han, "ShopMiner: Mining customer shopping behavior in physical clothing stores with passive RFIDs," in *Proc. ACM Conf. Embedded Netw. Sens. Syst.*, 2015, pp. 113–125.
[29] L. M. Ni, Y. Liu, Y. C. Lau, and A. P. Patil, "LANDMARC: Indoor location sensing using active RFID," *Wireless Netw.*, vol. 10, no. 6, pp. 701–710, 2004.
[30] C. Wang, H. Wu, and N.-F. Tzeng, "RFID-based 3-D positioning schemes," in *Proc. IEEE INFOCOM*, 2007, pp. 1235–1243.
[31] S. Azzouzi, M. Cremer, U. Dettmar, R. Kronberger, and T. Knie, "New measurement results for the localization of UHF RFID transponders using an angle of arrival (AoA) approach," in *Proc. IEEE Int. Conf. RFID*, 2011, pp. 91–97.
[32] J. Wang and D. Katabi, "Dude, where's my card?: RFID positioning that works with multipath and non-line of sight," in *Proc. ACM SIGCOMM Conf.*, 2013, pp. 51–62.
[33] R. Miesen, F. Kirsch, and M. Vossiek, "Holographic localization of passive UHF RFID transponders," in *Proc. IEEE Int. Conf. RFID*, 2011, pp. 32–37.
[34] L. Shangguan, Z. Yang, A. X. Liu, Z. Zhou, and Y. Liu, "Relative localization of RFID tags using spatial-temporal phase profiling," in *Proc. 12th USENIX Conf. Netw. Syst. Design Implementation*, 2015, pp. 251–263.
[35] Accessed: Aug. 23, 2019. [Online]. Available: http://www.eaibot.com/public/product/dashgo
[36] Accessed: Aug. 23, 2019. [Online]. Available: https://www.mathworks.com/help/matlab/ref/unwrap.html
[37] Accessed: Aug. 23, 2019. [Online]. Available: https://cdn.thomasnet.com/ccp/10014548/223252.pdf
[38] EPCglobal, Low Level Reader Protocol (LLRP), 2010. [Online]. Available: https://www.gs1.org/standards/epc-rfid/llrp/1-1-0
[39] A. Zhao, G. Tian, and J. Zhang, "IQ signal based RFID sensors for defect detection and characterisation," *Sens. Actuators A: Phys.*, vol. 269, pp. 14–21, 2018.
[40] M. Omer and G. Tian, "Indoor distance estimation for passive UHF RFID tag based on RSSI and RCS," *Meas.*, vol. 127, pp. 425–430, 2018.
[41] T. Wei and X. Zhang, "Gyro in the air: Tracking 3D orientation of batteryless Internet-of-Things," in *Proc. 22nd Annu. Int. Conf. Mobile Comput. Netw.*, 2016, pp. 55–68.
[42] J. Zhang, Y. Lyu, J. Patton, S. C. G. Periaswamy, and T. Roppel, "BFVP: A probabilistic UHF RFID tag localization algorithm using Bayesian filter and a variable power RFID model," *IEEE Trans. Ind. Electron.*, vol. 65, no. 10, pp. 8250–8259, Oct. 2018.
[43] E. DiGiampaolo and F. Martinelli, "A robotic system for localization of passive UHF-RFID tagged objects on shelves," *IEEE Sensors J.*, vol. 18, no. 20, pp. 8558–8568, Oct. 2018.

Xiulong Liu received the BE and PhD degrees from the Dalian University of Technology, Dalian, China, in 2010 and 2016, respectively. He is currently a professor with the College of Intelligence and Computing, Tianjin University, China. He also worked as a visiting researcher with Aizu University, Japan, a postdoctoral fellow with The Hong Kong Polytechnic University, Hong Kong, and a postdoctoral fellow with the School of Computing Science, Simon Fraser University, Canada. His research interests include wireless sensing and communication, indoor localization, networking, etc. His research papers were published in many prestigious journals and conferences including the *IEEE/ACM Transactions on Networking*, *IEEE Transactions on Mobile Computing*, *IEEE Transactions on Computers*, *IEEE Transactions on Parallel and Distributed Systems*, *IEEE Transactions on Communications*, INFOCOM, and ICNP, etc.

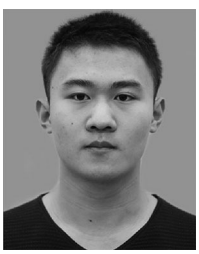

Jiuwu Zhang received the BE degree from the Hebei University of Technology, Hongqiao, China, in 2017. He is currently working toward the master's and PhD degrees at Tianjin University. His research interests include RFID technologies and wireless sensor networks.

Shan Jiang received the BE degree from Sun Yat-sen University, Guangzhou, China, in 2014. He is currently working toward the PhD degree in the Department of Computing, Hong Kong Polytechnic University, Hong Kong, China. His research interests include distributed computing, multi-robot system, and blockchain.

Yanni Yang received the BE and MSc degrees from the Ocean University of China, Qingdao, China, in 2014 and 2017, respectively. She is currently working toward the PhD degree in the Department of Computing, Hong Kong Polytechnic University, Hong Kong, China. Her research interests include wireless human sensing, pervasive, and mobile computing.

Keqiu Li received the bachelor's and master's degrees from the Department of Applied Mathematics, Dalian University of Technology, Dalian, China, in 1994 and 1997, respectively, and the PhD degree from the Graduate School of Information Science, Japan Advanced Institute of Science and Technology, Nomi, Japan, in 2005. He is currently a full professor, the dean of the College of Intelligence and Computing, Tianjin University, China. He is the recipient of National Science Foundation for Distinguished Young Scholars of China. He keeps working on the topics of mobile computing, datacenter, and cloud computing. He has more than 150 papers published on prestigious journals or conferences such as the *IEEE/ACM Transactions on Networking*, *IEEE Transactions on Parallel and Distributed Systems*, *IEEE Transactions on Computers*, *IEEE Transactions on Mobile Computing*, INFOCOM, ICNP, etc.

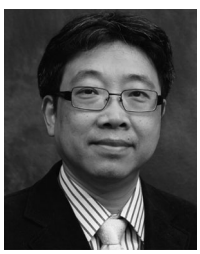

Jiannong Cao is currently a chair professor with the Department of Computing, Hong Kong Polytechnic University, Hong Kong. He is also the director of the Internet and Mobile Computing Lab in the department and the director of the University's Research Facility in Big Data Analytics. His research interests include parallel and distributed computing, wireless sensing and networks, pervasive and mobile computing, and big data and cloud computing. He has coauthored five books, co-edited nine books, and published more than 500 papers in major international journals and conference proceedings. He received best paper awards from conferences including DSAA'2017, IEEE SMARTCOMP 2016, ISPA 2013, etc. He is a fellow of the IEEE.

Jiangchuan Liu received the BEng (cum laude) degree from Tsinghua University, Beijing, China, in 1999, and the PhD degree from the Hong Kong University of Science and Technology, Hong Kong, in 2003. He is currently a full professor (with University Professorship) with the School of Computing Science, Simon Fraser University, British Columbia, Canada. He is a steering committee member of the *IEEE Transactions on Mobile Computing*, and associate editor of the *IEEE/ACM Transactions on Networking*, *IEEE Transactions on Big Data*, and *IEEE Transactions on Multimedia*. He is a co-recipient of the Test of Time Paper Award of IEEE INFOCOM (2015), ACM TOMCCAP Nicolas D. Georganas Best Paper Award (2013), and ACM Multimedia Best Paper Award (2012). He is a fellow of the IEEE, a Canadian Academy of Engineering fellow, and an NSERC E.W.R. Steacie memorial fellow.